Supporting Information: Structural polymorphism and luminescence properties of zinc(II) and cobalt(II) MOFs with rigid and flexible ligands

Pavel V. Burlak, Denis G. Samsonenko, Konstantin A. Kovalenko,* and Vladimir P. Fedin*

Nikolaev Institute of Inorganic Chemistry SB RAS, 3 Akad. Lavrentiev Av., 630090 Novosibirsk, Russian Federation

E-mail: k.a.kovalenko@niic.nsc.ru; cluster@niic.nsc.ru

Contents

1 Methods

^{1}H NMR spectra were recorded on a Bruker Advance 500 NMR spectrometer. **IR spectra** in the range 4000—400 cm^{-1} were recorded on a Bruker Scimitar FTS 2000 Fourier spectrometer. **Elemental analysis** was performed on a VarioMICROcube CHNS analyzer. Determination of the Zn/Co ratio was carried out on an Agilent 8800 ICP-MS. The samples were preliminarily dissolved in a mixture of nitric acid (high purity) and hydrogen peroxide, then diluted to the required concentration with the addition of 2% nitric acid (high purity). **XRD data** were obtained on a Shimadzu XRD 7000S powder diffractometer using Cu-Kα radiation, λ = 1.54056 Å for compounds **1**, **3**, **5**, **6**, and **7**, and Co-Kα radiation, λ = 1.78897 Å for compounds **2** and **4**. **Solid-state luminescence spectra** were recorded on a Horiba Jobin Yvon Fluorolog 3 spectrometer equipped with a 450 W Xe lamp and a PM-1073 PMT detector A Spectralon with a G8 integration sphere (GMP SA) was used to determine the luminescence quantum yield of solid samples.

Diffraction data for single-crystal of **1** were obtained at 140 K on an automated Agilent Xcalibur diffractometer equipped with an area AtlasS2 detector (graphite monochromator, λ(MoKα) = 0.71073 Å, ω-scans with a step of 0.25°). Integration, absorption correction, and determination of unit cell parameters were performed using the CrysAlisPro program package.[S1] Diffraction data for single-crystals of **2** and **3** were collected at 100 K on the 'Belok/XSA' beamline (λ = 0.79313 Å; φ-scans with a step of 1.0°) of the National Research Center 'Kurchatov Institute' (Moscow, Russian Federation) using a Rayonix SX165 CCD detector.[S2,S3] The data were indexed, integrated and scaled, absorption correction was applied using the XDS program package.[S4] The structures were solved by dual space algorithm (SHELXT[S5]) and refined by the full-matrix least squares technique (SHELXL[S6]) in the anisotropic approximation (except hydrogen atoms). Positions of hydrogen atoms of organic ligands were calculated geometrically and refined in the

riding model. The structure **3** contains void volume occupied with highly disordered guest water molecules, which could not be refined as a set of discrete atomic positions. The final composition of the compound **3** was defined according to PLATON/SQUEEZE procedure[S7] (206 e^- in 624 Å^3) and the data of element (C, H, N) analyses. The crystallographic data and details of the structure refinements are summarized in Table S1. CCDC 2358461–2358463 contain the supplementary crystallographic data for this paper. These data can be obtained free of charge from The Cambridge Crystallographic Data Center at https://www.ccdc.cam.ac.uk/structures/.

Table S1: Crystal data and structure refinement for **1**, **2**, and **3**

Identification code	**1**	**2**	**3**
Empirical formula	$C_{19}H_{19}N_5O_6Zn$	$C_{19}H_{19}CoN_5O_6$	$C_{19}H_{21}BrN_4O_5Zn$
Formula weight	478.76	472.32	530.68
Crystal system	*orthorhombic*	*orthorhombic*	*orthorhombic*
Space group	*Ibca*	*Ibca*	*Pccn*
a, Å	17.6280(6)	17.449(8)	32.038(17)
b, Å	15.8038(8)	15.828(3)	15.774(11)
c, Å	15.6293(14)	15.959(13)	17.871(6)
α	90°	90°	90°
β	90°	90°	90°
γ	90°	90°	90°
V, Å^3	4354.2(5)	4408(4)	9031(8)
Z	8	8	16
D_{calcd}, g/cm^3	1.461	1.424	1.561
μ, mm^{-1}	1.173	1.101	3.824
F(000)	1968	1944	4288
Crystal size, mm	$0.75 \times 0.17 \times 0.12$	$0.10 \times 0.05 \times 0.05$	$0.10 \times 0.06 \times 0.05$
θ range for data collection, deg	2.578–25.673	3.299–28.515	1.606–28.540
Index ranges	$-19 \leqslant h \leqslant 21$, $-18 \leqslant k \leqslant 19$, $-19 \leqslant l \leqslant 13$	$-20 \leqslant h \leqslant 20$, $-19 \leqslant k \leqslant 19$, $-19 \leqslant l \leqslant 19$	$-38 \leqslant h \leqslant 35$, $-19 \leqslant k \leqslant 19$, $-21 \leqslant l \leqslant 21$
Reflections collected / independent	8300 / 2061	13660 / 1983	57764 / 8235
Observed reflections $[I > 2\sigma(I)]$	1674	965	3711
R_{int}	0.0177	0.0953	0.1412
Goodness-of-fit on F^2	1.098	0.902	1.030
Final R indices $[I > 2\sigma(I)]$	$R_1 = 0.0537$, $wR_2 = 0.1650$	$R_1 = 0.0779$, $wR_2 = 0.2281$	$R_1 = 0.1342$, $wR_2 = 0.3947$
R indices (all data)	$R_1 = 0.0648$, $wR_2 = 0.1722$	$R_1 = 0.1374$, $wR_2 = 0.2727$	$R_1 = 0.2196$, $wR_2 = 0.4501$
Largest diff. peak and hole, e/Å^3	0.520 / −0.297	0.304 / −0.332	1.510 / −0.904
CCDC number	2358461	2358462	2358463

2 Crystal structures visualizations

2.1 Compound 1

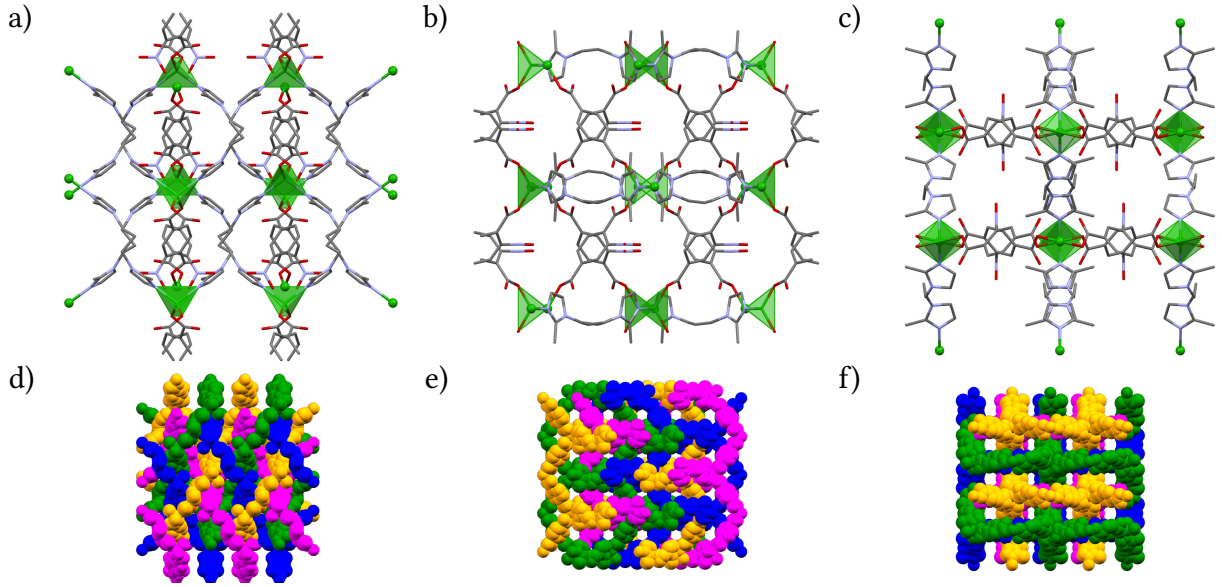

Figure S1: Structure of the compound **1**. Wireframe views along axes: a) *a*; b) *b*; c) *c*. Color scheme: Zn — green, C — grey, N — blue, O — red. Spacefill representation of the 4-fold interpenetration of the frameworks along axes: d) *a*; e) *b*; f) *c*.

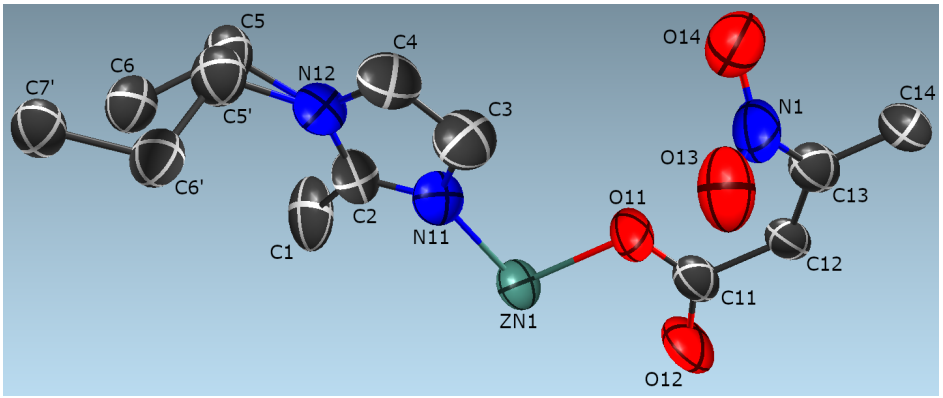

Figure S2: Asymmetric unit of the structure **1** in ellipsoids (50% probability) model. Color scheme: Zn — green, C — black, N — blue, O — red.

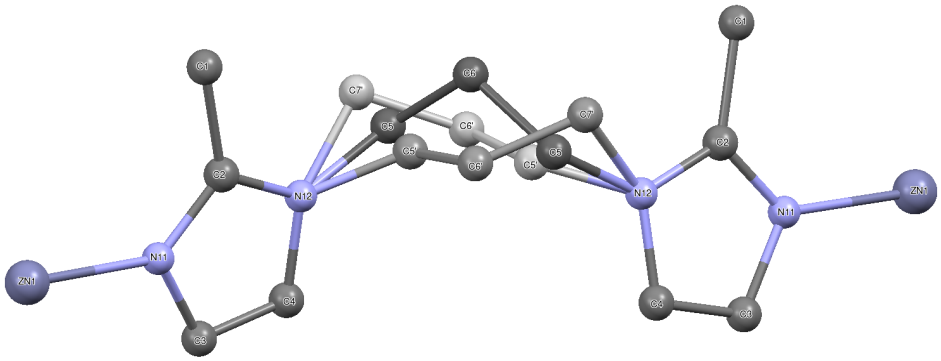

Figure S3: Disordering of bmip ligand in the compound **1**. See the description in the main text.

2.2 Compound 2

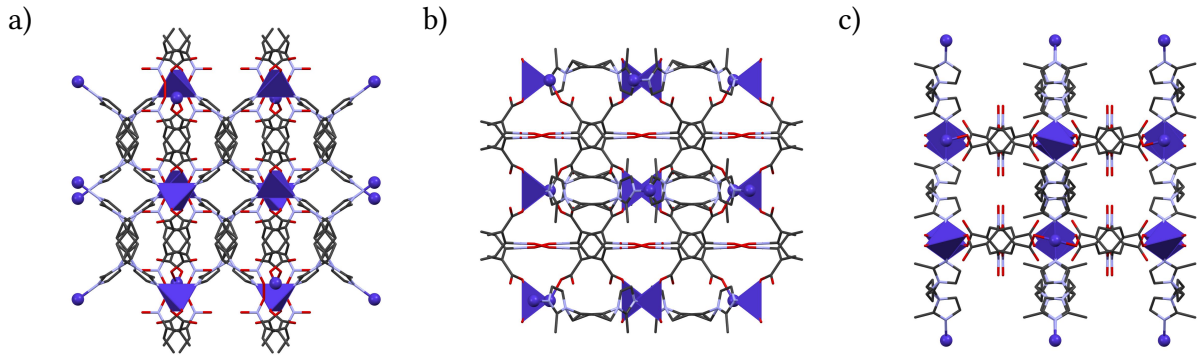

Figure S4: Structure of the compound **2**. Wireframe views along axes: a) *a*; b) *b*; c) *c*. Color scheme: Co — navy, C — grey, N — blue, O — red.

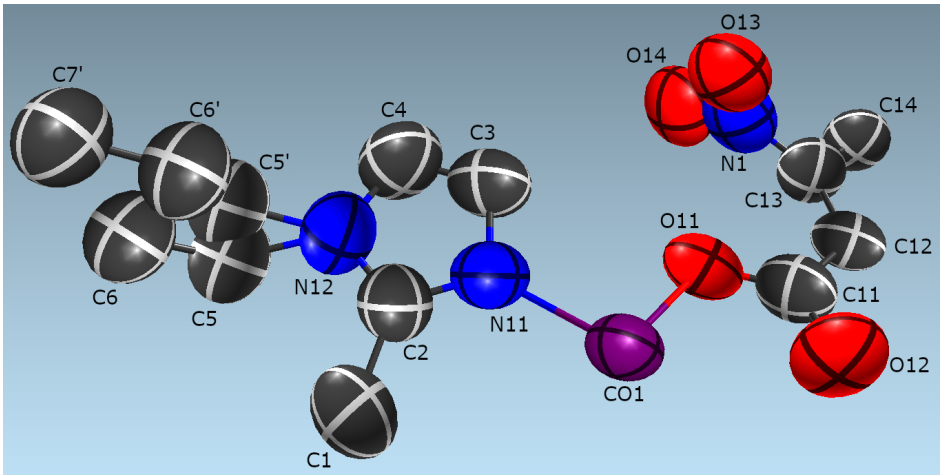

Figure S5: Asymmetric unit of the structure **2** in ellipsoids (50% probability) model. Color scheme: Co — purple, C — black, N — blue, O — red.

2.3 Compound 3

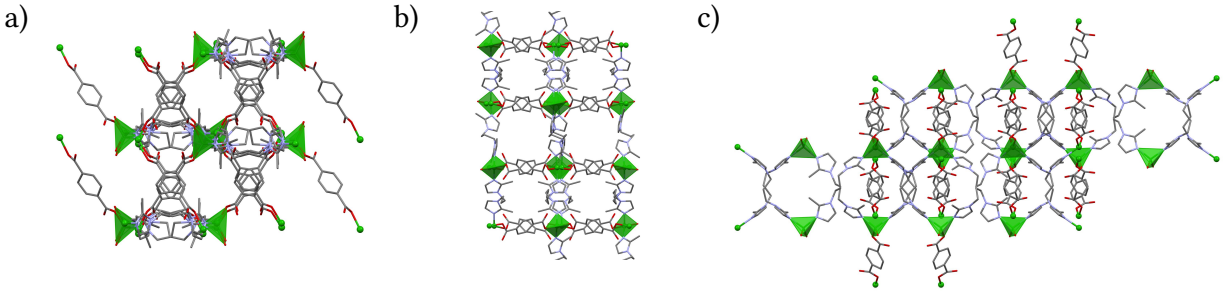

Figure S6: Structure of the compound **3**. Wireframe views along axes: a) *a*; b) *b*; c) *c*. Color scheme: Zn — green, C — grey, N — blue, O — red. Bromine atoms are not shown due to strong disordering.

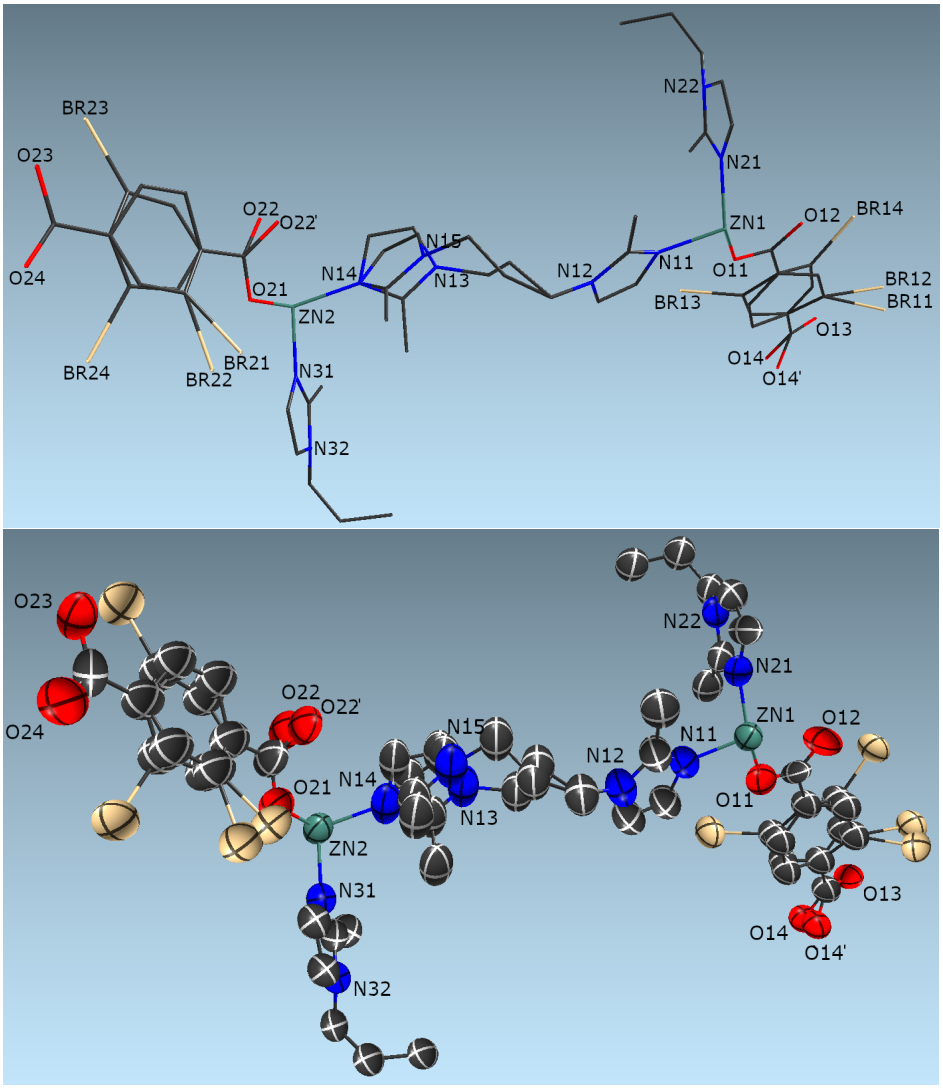

Figure S7: Asymmetric unit of the structure **3** in capped sticks (top) and ellipsoids (bottom) models (ellipsoids of 50% probability). Color scheme: Zn — green, C — black, N — blue, O — red.

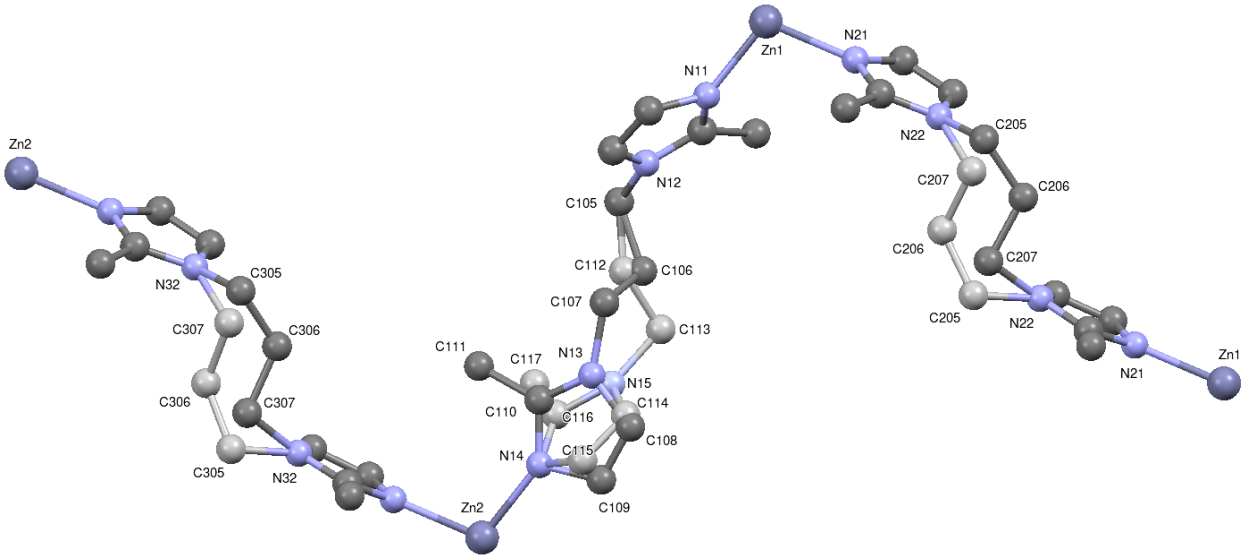

Figure S8: Disordering of bmip ligand in the compound **3**. See the description in the main text.

3 Characterization

3.1 Results of elemental analysis

Table S2: Elemental analysis of compounds obtained.

Compound	Composition	Calculated / Found			Zn/Co ratio found
		C, %	H, %	N, %	
1	$C_{19}H_{19}N_5O_6Zn$	47.7 / 47.6	4.0 / 3.9	14.6 / 14.5	—
2	$C_{19}H_{19}CoN_5O_6$	48.3 / 47.6	4.1 / 3.9	14.8 / 14.9	—
3	$C_{19}H_{19}BrN_4O_4Zn$	44.5 / 44.5	3.7 / 3.5	10.9 / 10.9	—
4	$C_{19}H_{19}BrCoN_4O_4$	45.1 / 45.1	3.8 / 3.9	11.1 / 11.5	—
5	$C_{19}H_{19}Co_{0.2}N_5O_6Zn_{0.8}$	47.8 / 47.8	4.0 / 3.9	14.7 / 14.7	4.03
6	$C_{19}H_{19}Co_{0.4}N_5O_6Zn_{0.6}$	47.9 / 47.8	4.0 / 3.9	14.7 / 14.6	3.1
7	$C_{19}H_{19}Co_{0.6}N_5O_6Zn_{0.4}$	48.1 / 48.0	4.0 / 3.6	14.7 / 14.7	2.05

4 Luminescence properties

4.1 Emission spectra

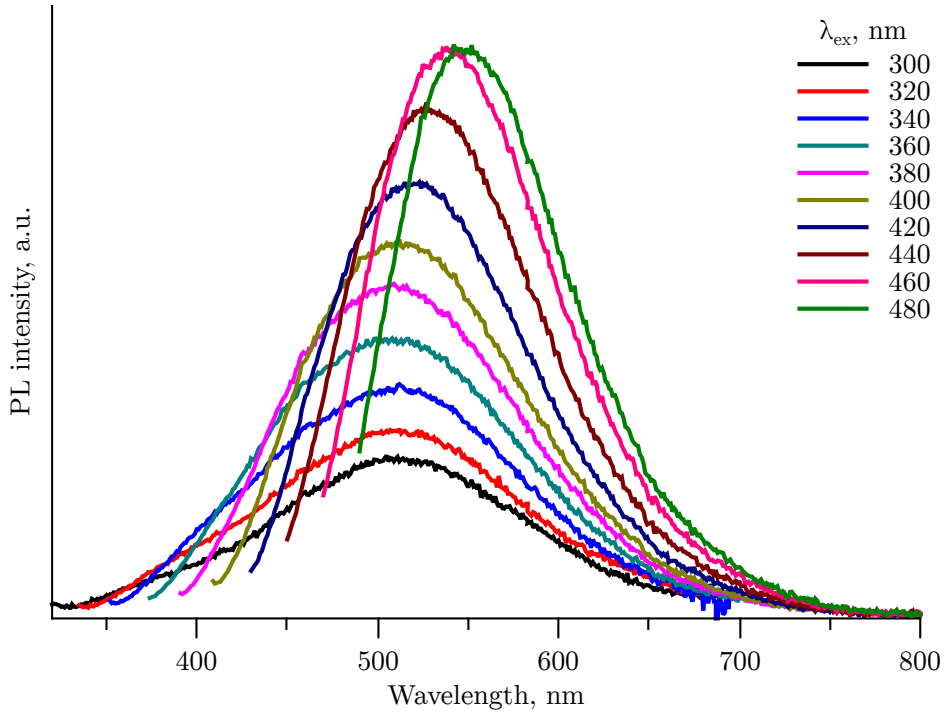

Figure S9: Wavelength excitation dependence of the emission spectra for bmip ligand.

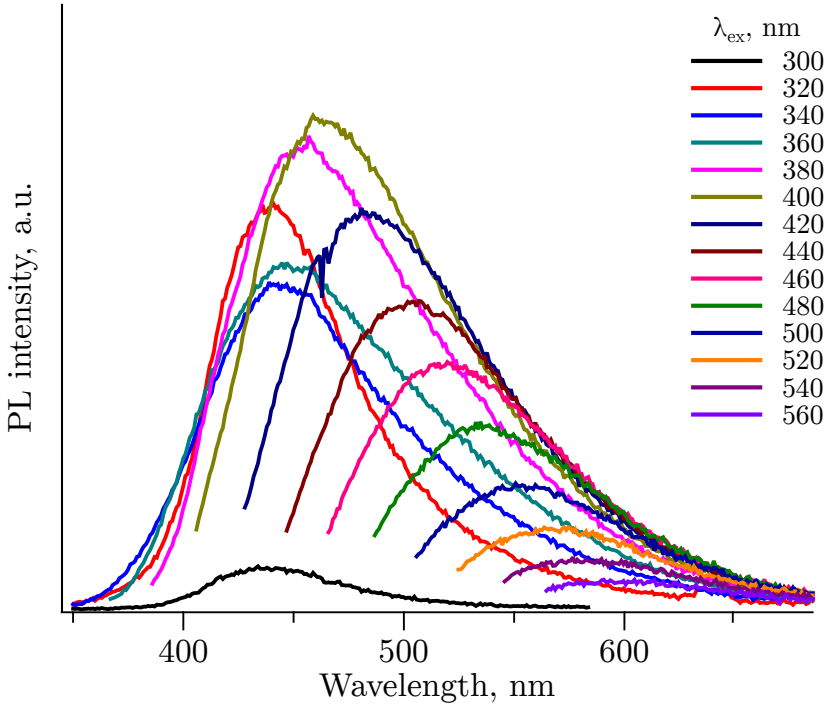

Figure S10: Wavelength excitation dependence of the emission spectra for compound **1**.

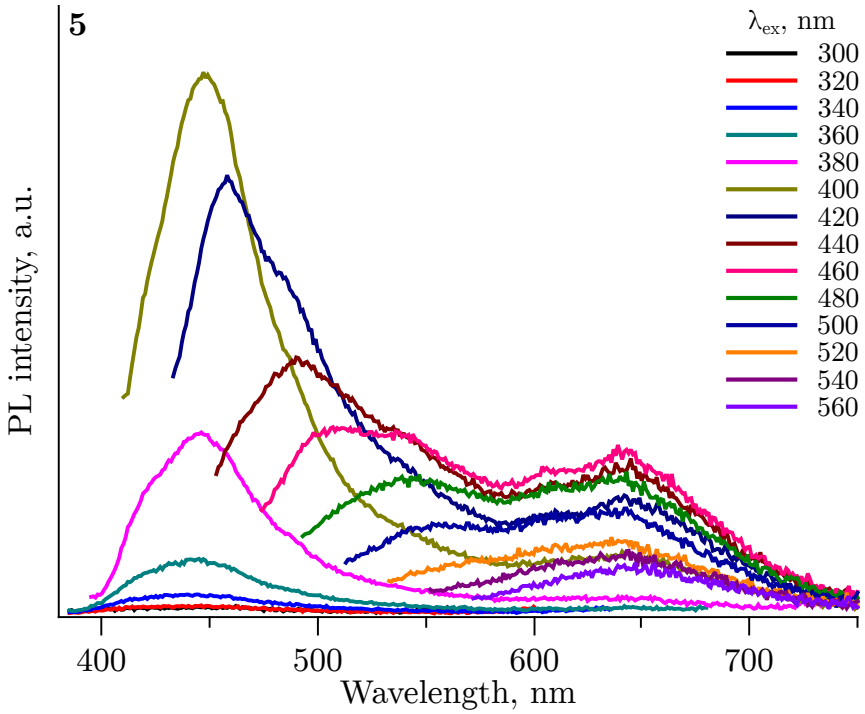

Figure S11: Wavelength excitation dependence of the emission spectra for compound **5**.

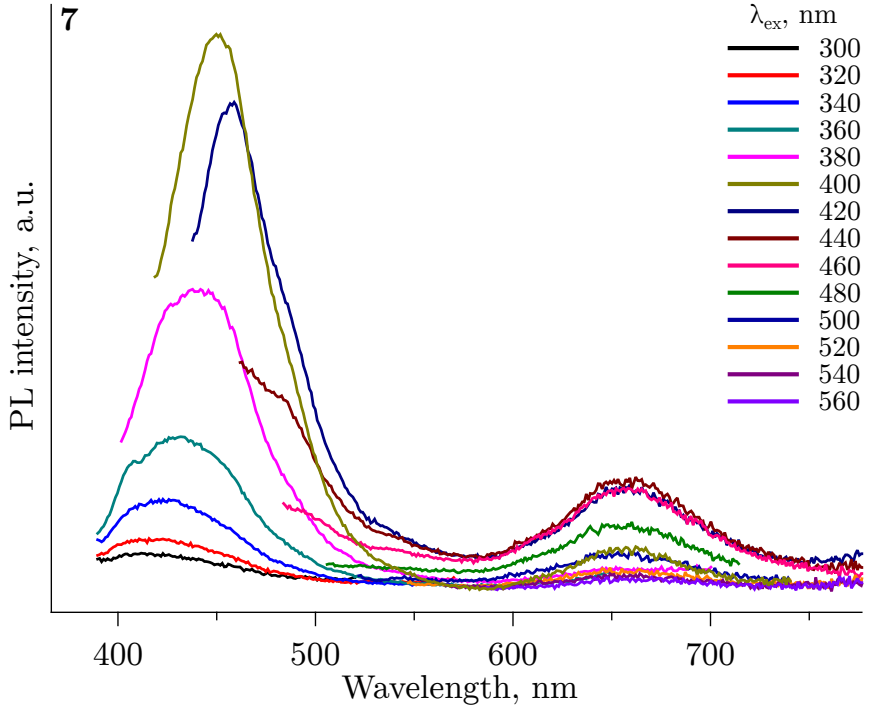

Figure S12: Wavelength excitation dependence of the emission spectra for compound **7**.

4.2 Chromaticity diagrams

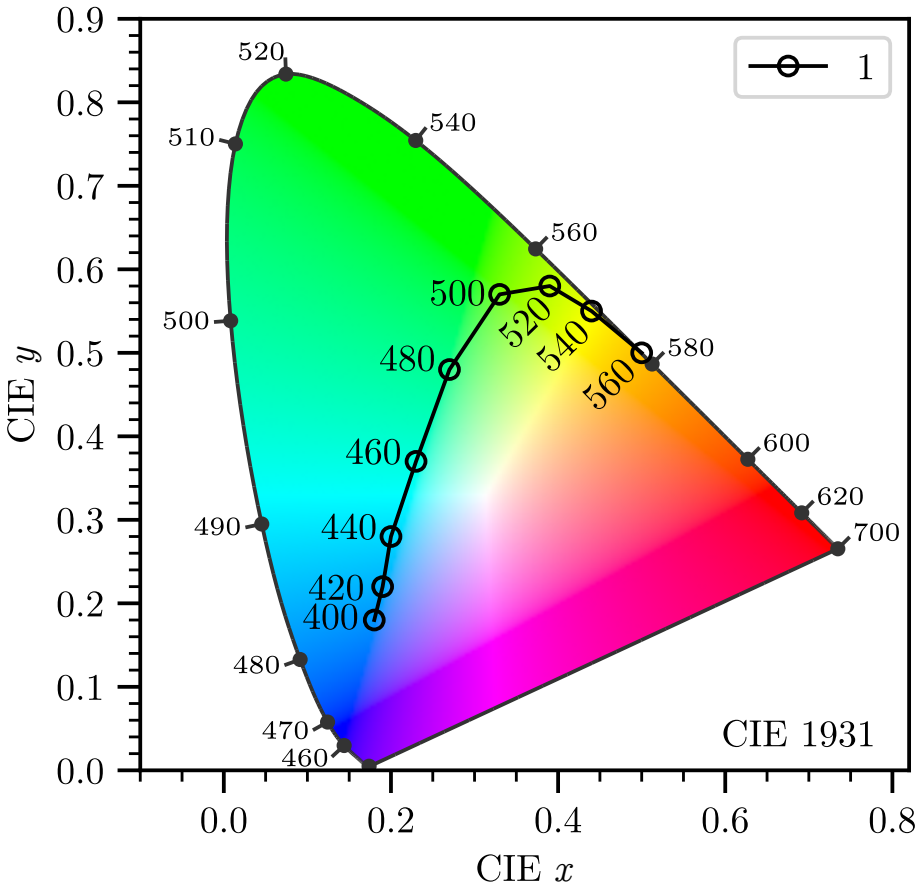

Figure S13: Wavelength excitation dependence of the PL chromaticity of **1** at 300 K.

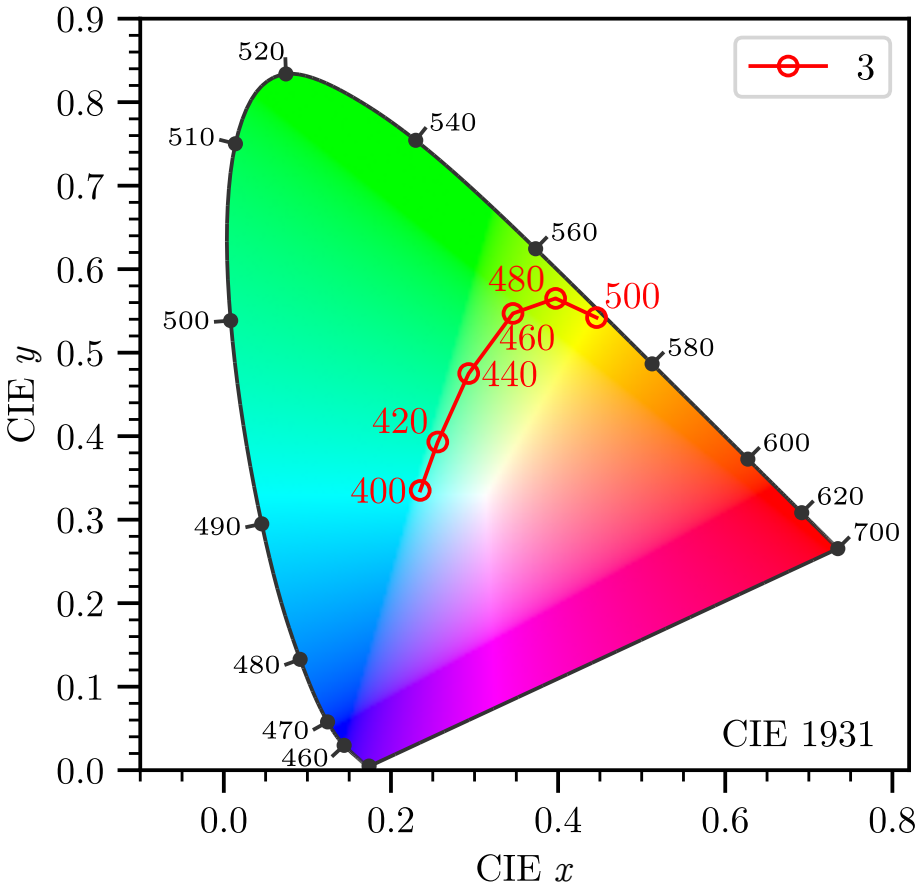

Figure S14: Wavelength excitation dependence of the PL chromaticity of **3** at 300 K.

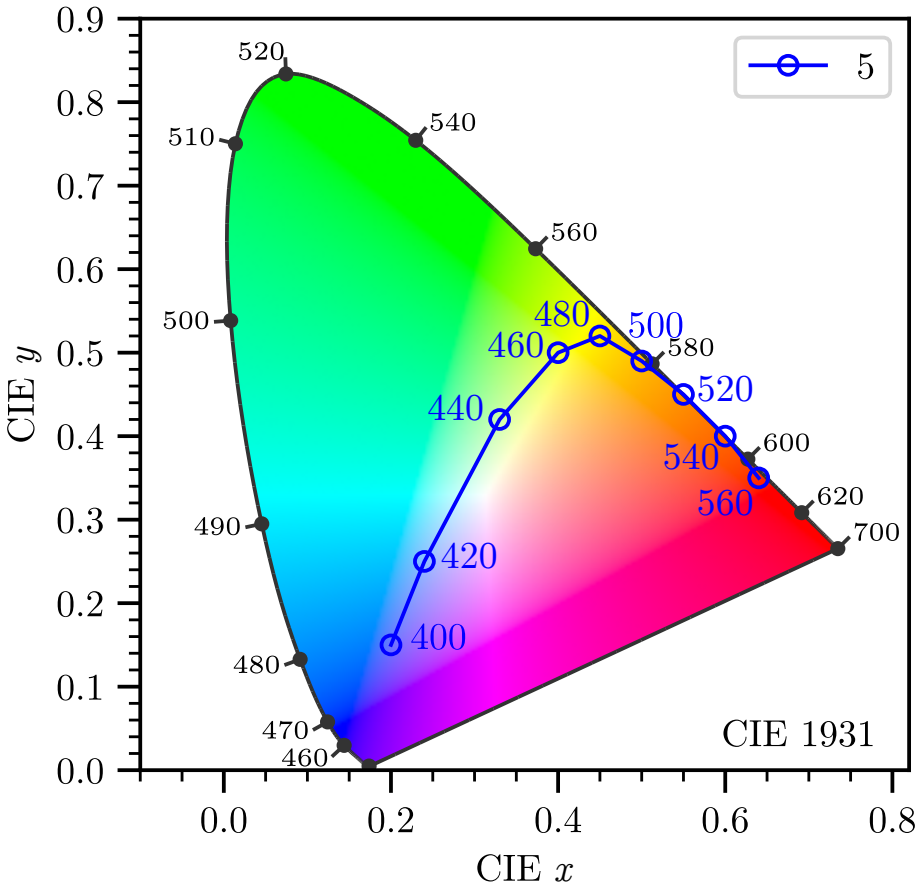

Figure S15: Wavelength excitation dependence of the PL chromaticity of **5** at 300 K.

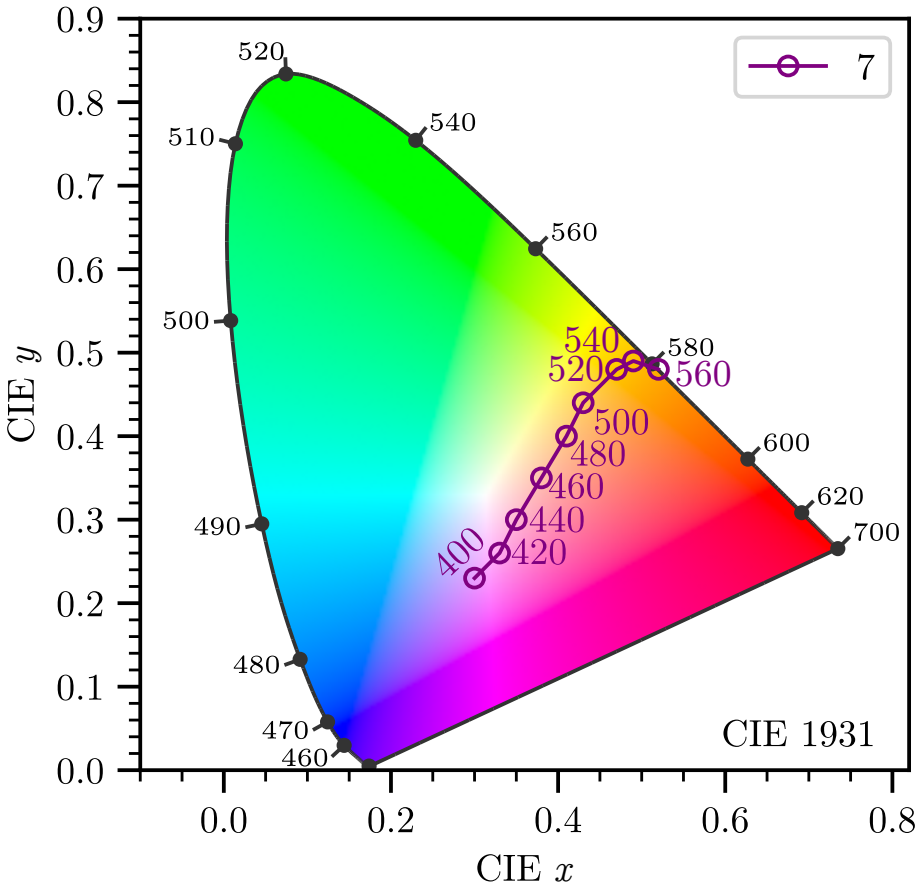

Figure S16: Wavelength excitation dependence of the PL chromaticity of **7** at 300 K.

References

(S1) CrysAlisPro Software System, Version 1.171.39.46. Rigaku Oxford Diffraction, Rigaku Corporation, Wrocław, Poland, 2018. 2018.

(S2) Svetogorov, R. D.; Dorovatovskii, P. V.; Lazarenko, V. A. Belok/XSA Diffraction Beamline for Studying Crystalline Samples at Kurchatov Synchrotron Radiation Source. *Cryst. Res. Technol.* **2020**, *55*, 1900184, DOI: 10.1002/crat.201900184.

(S3) Lazarenko, V. A.; Dorovatovskii, P. V.; Zubavichus, Y. V.; Burlov, A. S.; Koshchienko, Y. V.; Vlasenko, V. G.; Khrustalev, V. N. High-Throughput Small-Molecule Crystallography at the 'Belok' Beamline of the Kurchatov Synchrotron Radiation Source: Transition Metal Complexes with Azomethine Ligands as a Case Study. *Crystals* **2017**, *7*, 325, DOI: 10.3390/cryst7110325.

(S4) Kabsch, W. XDS. *Acta Crystallogr. Sect. D* **2010**, *66*, 125–132, DOI: 10.1107/S0907444909047337.

(S5) Sheldrick, G. M. *SHELXT* – Integrated Space-Group and Crystal-Structure Determination. *Acta Crystallogr. Sect. A* **2015**, *71*, 3–8, DOI: 10.1107/S2053273314026370.

(S6) Sheldrick, G. M. Crystal Structure Refinement with *SHELXL*. *Acta Crystallogr. Sect. C* **2015**, *71*, 3–8, DOI: 10.1107/S2053229614024218.

(S7) Spek, A. L. PLATON SQUEEZE: A Tool for the Calculation of the Disordered Solvent Contribution to the Calculated Structure Factors. *Acta Crystallogr. Sect. C* **2015**, *71*, 9–18, DOI: 10.1107/S2053229614024929.